Fluid models of impurity transport via drift wave turbulence

S. Futatani,[1,2] W. Horton,[2] S. Benkadda,[1] I. O. Bespamyatnov,[3] and W. L. Rowan[3]
[1]*International Institute for Fusion Science, CNRS—Université de Provence, Case 321, 13397 Marseille Cedex 20, France*
[2]*Institute for Fusion Studies, University of Texas at Austin, Austin, Texas 78712, USA*
[3]*Fusion Research Center, The University of Texas at Austin, Austin, Texas 78712, USA*

(Received 22 January 2010; accepted 25 May 2010; published online 26 July 2010)

Turbulent transport due to drift waves is a critical issue for fusion physics across all magnetic confinement geometries. Three-component fluid equations are used to find the eigenmodes and eigenfrequencies of a nonuniform, magnetized plasma with a four dimensional fluctuation vector composed of fluctuations of the electron density, the working gas ion density, the impurity density, and the electrostatic plasma potential. This structure of the eigenmodes and eigenvectors is shown for two collisionality regimes: (i) the collisional drift waves appropriate for the scrape-off-layer and the edge plasma in limiter discharges and (ii) the trapped electron mode taken in the limit of a Terry–Horton fluid description for the core plasma. From the eigenmodes and eigenvectors the part of the density and potential fluctuations that are out-of-phase is computed. The quasilinear particle fluxes are analyzed as a function of the power spectrum of the plasma potential fluctuations and the gradient parameters characterizing the Ohmic, H, and internal transport barrier confinement modes. A reversal in a direction of impurity flux is observed by changing the sign of the impurity density gradient length. After reversal, the impurity flux is directed outward and it is a favorable for fusion plasmas. © *2010 American Institute of Physics*. [doi:10.1063/1.3459062]

I. INTRODUCTION

Impurity transport is an important issue for fusion plasmas. Impurity accumulation in the core may lead to detrimental radiated power losses from high Z impurities and fuel dilution from both high and low Z impurities. Even so, impurities are unavoidable. They appear in the plasma due to ablation of walls due to plasma heat flux, wall erosion due to escaping fast ions, and intentional introduction to produce edge localized radiation for a continuous heat exhaust. The impurity elements are wide ranging and include both high and low Z. Argon may be injected to facilitate heat exhaust. The vacuum vessel walls may be sheathed in low Z elements such as carbon and beryllium and high Z elements such as tungsten. Different sections of the wall have different material requirements so that both high and low Z elements will be used. Indeed, there is already experimental evidence that plasma performance will be affected by materials choice: In JET enhanced performance with low effective charge $Z_{\mathrm{eff}}<2$ was obtained by changing the facing components from graphite to beryllium.[1] Although such results are clearly important in their own right, their optimum impact will come only after they are understood, they must be understood in terms of the underlying physics. It is crucial to understand the ramifications of these material choices for ITER plasma[2] and the transport of both high and low Z impurities using as transparent an explanation as practical.

We study how the collisional and trapped electron drift wave dynamics is modified by impurities and how the turbulence transports the impurities in a background of hydrogenic plasma with a density gradient. A system of fluid equations describing a generalized collisional drift wave turbulence for the hydrodynamic density and the impurity density is derived in the electrostatic approximation. The collisional regime is considered so the equations give a generalized form of the Hasegawa–Wakatani system of equations.[3] The trapped electron mode is modeled with a generalized form of the Terry–Horton system of equations which has a similar mathematical structure and is applied inside the separatrix.[4]

We show examples for a low Z impurity, boron, which is fully stripped, B^{5+}. Boron is one of the major impurities in Alcator C-Mod tokamak.[5] We characterize the level of the impurity density n_z with the Z_{eff} and limit $Z_{\mathrm{eff}}<1.5$ since higher Z_{eff} is not an interesting regime because it dilutes the hydrogenic fuel and prevents significant fusion power.

There are four space-time fields of interest, and the constraint of quasineutrality reduces the system to three free fields which are taken as the electron density, the hydrogenic ion density, and the impurity density. The condition of quasineutrality then determines the electrostatic field $\phi(x,t)$ and replaces the Poisson equation. Alternatively, one may view the three independent fields as the electrostatic potential and the two ion density fields, n_i and n_z, with the electron density determined by the quasineutrality condition

$$n_e(x,t) = n_i(x,t) + Zn_z(x,t). \tag{1}$$

The dynamics of the three density fields are determined by the Braginskii fluid equations in the approximation of low ion temperatures and finite electron temperature. The low ion temperature modeling simplifies the analysis considerably. We assume the plasma pressure is sufficiently low that the electrostatic approximation is valid.

The impurity is represented as a single field. This makes the theory more transparent and has an experimental realization. The theory best describes fully stripped ions, and its

ramifications can be explored with these ions on any device. Although the ion of interest may be different according to the temperature and density achieved, there will be typically one or more fully stripped ions to test this theory. We use comparison with recent Alcator C-Mod data to motivate the calculation parameters and assure that our theory remains within a consistent set of impurity profiles and plasma parameters.

In Sec. II we introduce the structure of the drift wave system of equations for one hydrogenic ion and one impurity species using the familiar Hasegawa–Wakatani model with cold ions and isothermal electrons to close the system of fluid equations. The section gives the nonlinear system of three partial differential equations from this analysis. In Sec. III we introduce the trapped electron fluid component to formulate the nonlinear and eigenvalue problem for the dissipative and collisionless models of the trapped electron instability in the absence of electron temperature gradients. In Sec. IV we present the linear analysis of the system of equations deriving a matrix formulation. The dispersion relations are calculated using the experimental data of Alcator C-Mod as input parameters. Then we show some examples for fully ionized boron with the plasma having an effect charge Z_{eff}. In Sec. V we present the quasilinear system of transport equations which are derived from the eigenvectors. The quasilinear flux which is calculated from the Alcator C-Mod parameters is also presented. In Sec. VI we analyze the variation of the impurity flux with increasing impurity density and the impurity profiles that are obtained in the steady state. In Sec. VII we present the conclusions and suggestions for future work and experiments.

II. DRIFT WAVES

The fluid model is used for mixed resistive drift wave turbulence. It is based on evolution equations for the densities and parallel velocity of electrons. We consider the isothermal equation of state to eliminate the temperature gradient driven modes. It is assumed that the magnetic field is uniform and in the z-direction, $\boldsymbol{B}=B_0\hat{\boldsymbol{e}}_z$. In the comparison work we analytically add the ion temperature gradient and impurity temperature gradient driving terms without the corresponding thermal field equations.

The Braginskii equations describe the evolution of fluid moments. The equations of the evolution of densities are

$$\frac{\partial n_s}{\partial t}+\nabla\cdot(n_s\boldsymbol{v}_s)=0, \tag{2}$$

where n_s and $\boldsymbol{v}_s$ are the density and the fluid velocity for each species s. Subscript s indicates species (e for electrons, i for ions, and z for impurities).

The evolution of fluid velocities is given by

$$n_s m_s\frac{d\boldsymbol{v}_s}{dt}=n_s e_s(\boldsymbol{E}+\boldsymbol{v}_s\times\boldsymbol{B})-\nabla p_s-\nabla\cdot\boldsymbol{\Pi}_s, \tag{3}$$

where p_s and $\boldsymbol{\Pi}_s$ are the pressure and the off-diagonal momentum stress tensor. The mass and charge of the particle are m_s and e_s for species s, respectively. Owing to the assumption of low ion temperatures only a small ion viscosity is kept from the ion momentum stress tensors.

Taking the outer product of $\boldsymbol{B}$ with Eq. (3) yields perpendicular components of drift velocity $\boldsymbol{v}_{s\perp}$ as $\boldsymbol{v}_{s\perp}=\boldsymbol{v}_E+\boldsymbol{v}_{s,*}+\boldsymbol{v}_{s,\mathrm{pol}}$, where the three velocity fields are defined as the $\boldsymbol{E}\times\boldsymbol{B}$ drift $\boldsymbol{v}_E=(\boldsymbol{E}\times\boldsymbol{B})/B^2$, the diamagnetic drift $\boldsymbol{v}_{s,*}=(1/e_s n_s)(\boldsymbol{B}/B^2)\times\nabla p_s$, and the polarization drift $\boldsymbol{v}_{s,\mathrm{pol}}=(m_s/e_s)(\boldsymbol{B}/B^2)\times(d\boldsymbol{v}_{s\perp}/dt)$. The electron polarization drift is negligible owing to the proportionality to the electron mass. The compressibilities of the velocities are $\nabla\cdot\boldsymbol{v}_E=0$, $\nabla\cdot\boldsymbol{v}_*=0$, and $\nabla\cdot\boldsymbol{v}_{s,\mathrm{pol}}=-(m_s/e_sB^2)(d/dt)\nabla^2\phi$.

After a short transit in which the pellet or the gas puff is ionized and the electrons stream over the magnetic surface, we have quasineutrality and the dynamics which are described by a reduced Eq. (2) as follows:

$$\begin{aligned}
&n_i+Zn_z=n_e,\\
&\frac{dn_i}{dt}+\mu_i\frac{m_i}{eB^2}\nabla^4\phi=\nabla\cdot\left(\frac{m_i n_i}{eB^2}\frac{d}{dt}\nabla\phi\right),\\
&\frac{dn_z}{dt}+\mu_z\frac{m_z}{eB^2}\nabla^4\phi=\nabla\cdot\left(\frac{m_z n_z}{ZeB^2}\frac{d}{dt}\nabla\phi\right),\\
&\frac{dn_e}{dt}+\frac{\omega_{De}}{k_y}\frac{\partial n_e}{\partial y}=\frac{1}{e}\nabla_\parallel\cdot J_\parallel.
\end{aligned} \tag{4}$$

The generalized Ohm's law gives

$$J_\parallel=\sigma_\parallel\left(E_\parallel+\frac{T_e}{en_e}\frac{\partial n_e}{\partial z}\right)=\sigma_\parallel\left(-\frac{\partial\phi}{\partial z}+\frac{T_e}{en_e}\frac{\partial n_e}{\partial z}\right). \tag{5}$$

We define the total derivative by the advective portion due to $\boldsymbol{v}_E$, giving $d/dt=(\partial/\partial t)+\boldsymbol{v}_E\cdot\nabla$. The second term on the lhs of Eq. (4) has μ_i and μ_z which are the viscosities of ions and impurities, respectively. The electron temperature is T_e and η is the electron resistivity. The resistivity $\eta=1/\sigma_\parallel$ is taken as a function of T_e which is constant in this isothermal model. The ion temperatures are assumed to be low enough that the ion thermal terms such as the ion diamagnetic drift and ion momentum stress tensor are negligible. The definition of effective charge Z_{eff} that determines the resistivity η and the impurity dilution of the hydrogenic fusion fuel component is

$$Z_{\mathrm{eff}}=\frac{n_i+Z^2n_z}{n_i+Zn_z},\quad 1\le Z_{\mathrm{eff}}<Z. \tag{6}$$

For boron (B) ($Z=5$), the $Z_{\mathrm{eff}}=1.2$ limit corresponds to the reasonably small concentration $n_z/n_e=1\times10^{-2}$.

III. TRAPPED ELECTRON MODE

A. Kinetic trapped electron mode theory

Plasma collisionality is low inside the separatrix so the collisional drift wave evolves into the collisional trapped electron mode.[6] In the core plasma, low collisionality transforms the instability in the collisionless trapped electron mode (CTEM). We model the toroidal magnetic field variation as

$$B = B_0\left(1 - \frac{r}{R}\cos\theta\right). \tag{7}$$

Small aspect ratio $\epsilon = r/R \ll 1$ is considered here, and the fraction of trapped particles f_t can then be reduced by

$$f_t = \frac{\text{trapped electrons}}{\text{total electrons}} = \left(\frac{B_{\max}}{B_{\min}} - 1\right)^{1/2} = \left(\frac{1+\epsilon}{1-\epsilon} - 1\right)^{1/2} = 1 - f_p, \tag{8}$$

where f_p is the fraction of passing electrons.

The trapped electron instability is derived from the drift-kinetic equation for the nonadiabatic electron distribution function $h_{\boldsymbol{k},\omega}(E,\mu,r,\theta)$ which satisfies

$$\nu(v)\frac{\partial}{\partial\mu}(1-\mu^2)\frac{\partial h_e}{\partial\mu} + i\left(\omega - \omega_{De}\frac{v^2}{v_e^2} - k_\parallel v\mu\right)h_e = i\left\{\omega - \omega_*\left[1 + \eta_e\left(\frac{v^2}{v_e^2} - \frac{3}{2}\right)\right]\right\}, \tag{9}$$

where $\nu(v) = \nu_e(v_e/v)^3$, $\omega_{De} \sim \omega_*(2L_n/R) = 2\omega_*\epsilon_n$, $\eta_e = d\log T_e/d\log n_e$, $v_e = (2T_e/m_e)^{1/2}$, and $\mu = v_\parallel/v$.

There are three driving terms for the out-of-phase part of $h_{e,\boldsymbol{k},\omega}$ that give the particle fluxes. The driving terms are $G_1 = R/L_{en}$, $G_2 = R/L_{Te}$, and $G_3 = 2\cos\theta/R$. The growth/damping rate γ_k is a function of the G_α which may be expressed as

$$\gamma_k = \sum_{\alpha=1}^{3}\left(\frac{d\gamma_k}{dG_\alpha}G_\alpha\right). \tag{10}$$

The solution of the drift-kinetic equation Eq. (9) divides into a low energy collisional part where

$$\frac{v}{v_e} \ll \left(\frac{\nu_e}{k_\parallel v_e \epsilon^{3/2}}\right)^{1/4} \tag{11}$$

and

$$h_{e0}(v) = \frac{\omega - \omega_*\{1 + \eta_e(v^2/v_e^2 - 3/2)\}}{\omega - \omega_{De}v^2/v_e^2 + i(\nu_e/\epsilon)(v_e/v)^3}. \tag{12}$$

In the core of the plasma the effective collisionality ν_{*e} of the high energy electrons is small,

$$\nu_{*e} = \nu_e qR/(\epsilon^{3/2}v_e) < 1, \tag{13}$$

where we use the depth of the mirror well $\Delta B/B \sim 2\epsilon$ in Eq. (8).

The high energy solution of the electron kinetic equation, Eq. (9), gives fluctuating δf_e,

$$\delta f_e = f_M\frac{e}{T_e}\left\{\phi - \frac{1}{\tau}\int\frac{ds'}{v_\parallel}\phi(s')\frac{\omega - \omega_{*e}}{\omega - \omega_{De} + i\nu_{\text{eff}}}\right\}, \tag{14}$$

where $\int(ds'/v_\parallel)$ is the bounce time period. For the trapped particle instability we have the orbit integral which is discontinuous integral as follows:

$$\frac{1}{\tau}\int\frac{ds'}{v_\parallel}\phi = 0 \quad \text{(passing electrons)} \qquad \simeq \phi \quad \text{(trapped electrons)} \tag{15}$$

due to phase mixing of ϕ over the irrational toroidal field lines.

B. Collisionless trapped electron mode and dissipative trapped electron mode

The details of the trapped particle mode analysis are given in Ref. 7. From Eqs. (14) and (15) we derive the passing δn_p and trapped particles densities,

$$\delta n_p = \int d^3v\,\delta f_p = f_p\frac{n_e e\phi}{T_e}, \tag{16}$$

$$\delta n_t = \int d^3v\,\delta f_t = f_t\frac{n_e e\phi}{T_e}\left[1 - \frac{\omega - \omega_{*e}}{\omega - \omega_{De} + i\nu_{\text{eff}}}\right]. \tag{17}$$

There are two regimes of trapped electron modes: the collisionless trapped electron mode (CTEM) and the dissipative trapped electron mode (DTEM). For the CTEM, that is $\nu_{\text{eff}} \ll \omega_{De}$, we have

$$\frac{\delta n_e}{n_e} = \frac{n_e e\phi}{T_e}\{1 + i\pi f_t\langle(\omega - \omega_{*e})[\delta(\omega - \omega_{De})]\rangle\}. \tag{18}$$

For the DTEM, that is $\nu_{\text{eff}} \gg |\omega| \sim \omega_{De}$, we have

$$\frac{\delta n_e}{n_e} = \frac{n_e e\phi}{T_e}\left[1 + if_t\frac{\omega - \omega_{*e}}{\nu_{\text{eff}}}\right]. \tag{19}$$

These formulas are used in the Terry–Horton model as explained in Ref. 8.

For the collisionless regime $\nu_{\text{eff}} \ll \omega_{*e}$, the nonlinear dynamical equation for the passing electron mode is

$$\delta n_p = \frac{en_p}{T_e}\phi_k,$$

where $\delta n_p = n_p - n_{p0}$ and is linear. The dissipative limit is

$$\frac{\partial n_t}{\partial t} + \boldsymbol{v}_E\cdot\nabla n_t = -\nu_{\text{eff}}(n_t - n_{t0}) \tag{20}$$

given by $n_{t0} = f_t n_e$. The fluctuating trapped electron density δn_t is

$$(-i\omega+\nu_{\mathrm{eff}})\delta n_t+\frac{-ik_y\phi}{B}\frac{dn_t}{dr}=0. \tag{21}$$

For the transition from the collisional regime to the hot core plasma for $|\omega_{De}|>\nu_{\mathrm{eff}}$ the dissipation is replaced with $\nu_{\mathrm{eff}}\rightarrow c_D|\omega_{De}|$, where the constant c_D is chosen to be in agreement with gyrokinetic codes.

The nonlinear fluid trapped electron mode is described by

$$\begin{aligned}
&\frac{dn_i}{dt}+\mu_i\frac{m_i}{eB^2}\nabla^4\phi=\nabla\cdot\left(\frac{m_in_i}{eB^2}\frac{d}{dt}\nabla\phi\right),\\
&\frac{dn_z}{dt}+\mu_z\frac{m_z}{eB^2}\nabla^4\phi=\nabla\cdot\left(\frac{m_zn_z}{ZeB^2}\frac{d}{dt}\nabla\phi\right),\\
&n_e=-n_ef_p\frac{e\phi}{T_e}+Z\delta n_z+n_{t0},\\
&\frac{d\delta n_t}{dt}+\frac{\omega_{De}}{k_y}\frac{\partial\delta n_t}{\partial y}=-\nu_{\mathrm{eff}}\delta n_t.
\end{aligned} \tag{22}$$

IV. LINEAR EIGENMODES ANALYSIS

A. Matrix equations for fluctuations

Linearization and Fourier decomposition of equations in the previous section, assuming a modal dependence of the type $\exp i(\boldsymbol{k}\cdot\boldsymbol{r}-\omega t)$, lead to a dispersion relation. In the linearized system, the unstable modes are the only remaining modes after the system evolves for a finite time. They are characterized by a real frequency ω_k and a growth rate γ_k: $\omega=\omega_k+i\gamma_k$.

Now we define the eigenmodes and eigenvectors of the linearized dynamical equations. In a linearization process of Eq. (4), we look for spectral solutions of the form of $\exp(i\boldsymbol{k}\cdot\boldsymbol{x}-i\omega t)$ and derive the following 4×4 matrixes $\boldsymbol{M}_{\mathrm{CDW}}(\boldsymbol{k},\omega)$ for the field vector $\boldsymbol{X}^T=(\delta n_i/n_e,\delta n_z/n_e,\times\delta n_e/n_e,e\phi/T_e)$, thus one can express the set of Eq. (4) by

$$\boldsymbol{M}_{\mathrm{CDW}}(\boldsymbol{k},\omega)\boldsymbol{X}\left(\frac{\delta n_i}{n_e},\frac{\delta n_z}{n_e},\frac{\delta n_e}{n_e},\frac{e\phi}{T_e}\right)=\boldsymbol{0}. \tag{23}$$

The matrix $\boldsymbol{M}_{\mathrm{CDW}}(\boldsymbol{k},\omega)$ of the set of Eq. (4) is defined as follows:

$$\boldsymbol{M}_{\mathrm{CDW}}(\omega,\boldsymbol{k})=\begin{bmatrix}1 & Z & -1 & 0\\ -i\omega & 0 & 0 & -i\omega_{*i}-i(\omega+i\mu_ik_\perp^2)k_\perp^2\rho_{s,i}^2\\ 0 & -i\omega & 0 & -i\omega_{*z}-i(\omega+i\mu_zk_\perp^2)k_\perp^2\rho_{s,z}^2\\ 0 & 0 & -i\omega+k_\parallel^2D_\parallel+i\omega_{De} & i\omega_{*e}-k_\parallel^2D_\parallel\end{bmatrix}. \tag{24}$$

The matrix $\boldsymbol{M}_{\mathrm{CDW}}(\boldsymbol{k})$ contains the three drift wave frequencies and the curvature drift frequency which are

$$\begin{aligned}
&\omega_{*i}=k_y\frac{T_e}{eB}\frac{1}{n_e}\frac{dn_i}{dx},\\
&\omega_{*z}=k_y\frac{T_e}{ZeB}\frac{1}{n_e}\frac{dn_z}{dx},\\
&\omega_{*e}=-k_y\frac{T_e}{eB}\frac{1}{n_e}\frac{dn_e}{dx},
\end{aligned} \tag{25}$$

$$\omega_{De}=k_y\frac{2T_e}{eBR}\cos\theta.$$

From Eq. (25) and the charge neutrality condition we derive

$$\omega_{*e}+\omega_{*i}+Z^2\omega_{*z}=0. \tag{26}$$

In summary we have the system parameters

$$\begin{aligned}
&\rho_{s,i}^2=\frac{m_iT_e}{e^2B^2},\quad \rho_{s,z}^2=\frac{m_zT_e}{Ze^2B^2},\\
&D_\parallel=\frac{\sigma_\parallel T_e}{n_ee^2},\quad \sigma_\parallel=\frac{n_ee^2}{m_e\nu_e}.
\end{aligned} \tag{27}$$

Similarly, the trapped electron drift eigenvalue problem of Eq. (22) is given by the matrix which is given by

$$\boldsymbol{M}_{\mathrm{TEM}}(\omega,\boldsymbol{k})=\begin{bmatrix}1 & Z & -1 & -f_p\\ -i\omega & 0 & 0 & -i\omega_{*i}-i(\omega+i\mu_ik_\perp^2)k_\perp^2\rho_{s,i}^2\\ 0 & -i\omega & 0 & -i\omega_{*z}-i(\omega+i\mu_zk_\perp^2)k_\perp^2\rho_{s,z}^2\\ 0 & 0 & -i\omega+\nu_{\mathrm{eff}}+i\omega_{De} & i\omega_{*e}f_t\end{bmatrix}, \tag{28}$$

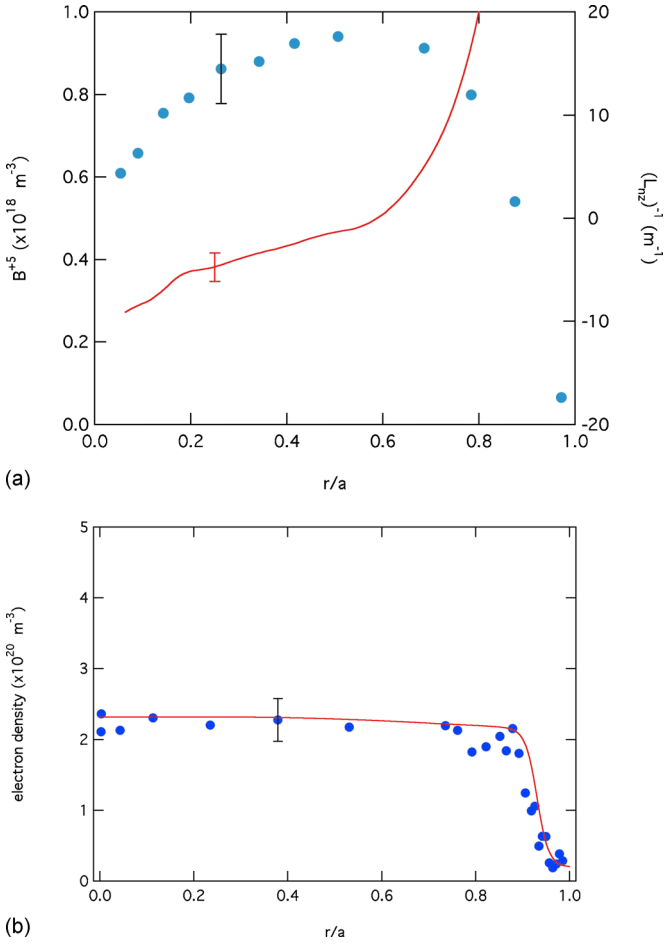

FIG. 1. (Color online) The density profiles and inverse density gradient scale lengths of boron B^{5+} during an H-mode of the Alcator C-Mod tokamak. (a) Measurement of B^{5+} density profile (solid circles) and the inverse gradient scale length L_{nz}^{-1} of B^{5+} density. (b) The measurement of electron density profile (solid circles) and the data fit (solid line). Typical error bars are indicated (Ref. 12).

and the field vector is $\boldsymbol{X}^T=(\delta n_i/\delta n_e, \delta n_z/\delta n_e, \delta n_{et}/\delta n_e, \times e\phi/T_e)$. Thus one can express the set of Eq. (22) by

$$\boldsymbol{M}_{\mathrm{TEM}}(\boldsymbol{k},\omega)\boldsymbol{X}\left(\frac{\delta n_i}{n_e},\frac{\delta n_z}{n_e},\frac{\delta n_{et}}{n_e},\frac{e\phi}{T_e}\right)=\boldsymbol{0}. \tag{29}$$

B. Dispersion relations

Measured H-mode B^{5+} profiles from Alcator C-Mod are shown in Fig. 1. This particular impurity density profile is peaked near $r/a=0.6$ and is hollow near the core $r/a=0.2$. Measurements at two different locations are used for the transport analysis $r/a=0.2$ and $r/a=0.6$. The impurity density gradient length, which is defined as $L_{nz}^{-1}=-\nabla n_z/n_z$, is negative at $r/a=0.2$, $L_{nz}=-0.18$ m<0, i.e., hollow impurity density profile. At the flattop of the profile, $r/a=0.6$, the impurity gradient length is positive and very large, $L_{nz}=1.43$ m>0, i.e., peaked impurity density profile. Viscosities of ions and impurities, μ_i and μ_z, respectively, are $\mu_i=3.55\times10^{-4}$ m^2/s and $\mu_z=1.1\times10^{-3}$ m^2/s. The analysis is applied to the two different normalized radii, $r/a=0.2$ and $r/a=0.6$. All relevant plasma parameters can be found in Table I.

The dispersion relations of the collisional drift wave model and the trapped electron model which are calculated from the determinant of Eqs. (24) and (28), respectively, are shown in Fig. 2. The dispersion relations are calculated using the determinant of the matrix M_{CDW} and M_{TEM}, which gives a cubic polynomial equation. The trapped electron modes are characterized by peaking of the frequency for $k_y\sim350$ m^{-1} and an exponential decrease for higher k_y values. In comparison to TEM, the collisional drift wave modes are characterized by slower peaking of the frequency for $k_y\sim600$ m^{-1} and slower exponential decrease. The curves of growth rate indicate that unstable modes exist in the trapped electron mode while the collisional drift wave is weakly unstable. Note that H-mode electron density profile of Alcator C-Mod experiment is closely flat, therefore, the collisional drift wave whose energy source is a density gradient is mostly stable. Thus, we have a lower and higher frequency mode of oscillations. The higher frequency mode is unstable for $k_y=900$ m^{-1} shown in Fig. 2. Figure 2 shows the trapped electron mode has a maximum growth rate at $k_y=350$ m^{-1}, where the frequency $\omega=7\times10^4$ rad/s.

V. EIGENVECTORS AND QUASILINEAR FLUXES

The eigenvalues and the eigenvectors of the linear modes of the impure plasma can be calculated from the matrices in Eqs. (24) and (28). The eigenvectors of the impurity drift wave matrix give the polarization of the fluctuations that determine the relative strength and direction of the impurity and hydrogenic ion transport. There is now an extra degree of freedom for the hydrogenic ion density owing to the motion of the impurity ions.

The full matrix $\boldsymbol{M}(\boldsymbol{k},\omega)$ given by Eq. (24), is decomposed into $\boldsymbol{M}(\boldsymbol{k},\omega)=\boldsymbol{A}(\boldsymbol{k})-i\omega\boldsymbol{B}(\boldsymbol{k})$. Here, the matrix $\boldsymbol{A}(\boldsymbol{k})$ and $\boldsymbol{B}(\boldsymbol{k})$ are defined as follows:

$$\boldsymbol{A}(\boldsymbol{k})=\begin{bmatrix}1 & Z & -1 & 0\\ 0 & 0 & 0 & i\omega_{*i}+\mu_i k_\perp^4\rho_{s,i}^2\\ 0 & 0 & 0 & i\omega_{*z}+\mu_z k_\perp^4\rho_{s,z}^2\\ 0 & 0 & k_\parallel^2 D_\parallel & i\omega_{*e}-k_\parallel^2 D_\parallel\end{bmatrix}, \tag{30}$$

$$\boldsymbol{B}(\boldsymbol{k})=\begin{bmatrix}0 & 0 & 0 & 0\\ 1 & 0 & 0 & k_\perp^2\rho_{s,i}^2\\ 0 & 1 & 0 & k_\perp^2\rho_{s,z}^2\\ 0 & 0 & 1 & 0\end{bmatrix}. \tag{31}$$

In terms of the $\boldsymbol{A}$ and $\boldsymbol{B}$ matrices the system linear fluctuation equations becomes

$$\boldsymbol{A}(\boldsymbol{k})\boldsymbol{X}=-i\omega\boldsymbol{B}(\boldsymbol{k})\boldsymbol{X}. \tag{32}$$

Carrying out the solution of the eigenvalue problem of Eq. (32) gives the eigenvectors X_α for each root ω_α, which is equivalent to the solution of the dispersion relation $D(\omega,k_x,k_y,k_\parallel)=\det\boldsymbol{M}=0$. Now we factor out the value of

TABLE I. Typical Alcator C-Mod tokamak plasma parameters.

	$r/a=0.2$	$r/a=0.6$
Major radius	$R=0.67$ m	$R=0.67$ m
Minor radius	$a=0.22$ m	$a=0.22$ m
Magnetic field	$B=5.4$ T	$B=5.4$ T
q-value	$q\sim 1.16$	$q\sim 1.84$
Electron temperature	$T_e=1258.8$ eV	$T_e=626.2$ eV
Electron density	$n_e=2.23\times 10^{20}$ m^{-3}	$n_e=2.21\times 10^{20}$ m^{-3}
Impurity density	$n_z=8.02\times 10^{17}$ m^{-3}	$n_z=9.5\times 10^{17}$ m^{-3}
Parallel wavenumber	$k_\parallel=\frac{0.5}{qR}\sim 0.6433$ m^{-1}	0.41 m^{-1}
Electron velocity	$v_e=\left(\frac{T_e}{m_e}\right)^{1/2}=1.49\times 10^7$ m s^{-1}	1.05×10^7 m s^{-1}
Sound velocity	$c_s=\left(\frac{T_e}{m_i}\right)^{1/2}=3.47\times 10^5$ m s^{-1}	2.45×10^5 m s^{-1}
Ion gyroradius	$\rho_s=c_s/\omega_{ci}=6.71\times 10^{-4}$ m	4.73×10^{-4} m
Electron parallel diffusion	$D_\parallel=\frac{v_e}{k_\parallel}=2.31\times 10^7$ m^2 s^{-1}	2.59×10^7 m^2 s^{-1}
Parallel diffusion rate	$\nu_\parallel=k_\parallel^2 D_\parallel=9.57\times 10^6$ rad s^{-1}	4.25×10^6 rad s^{-1}
Electron density gradient length	$L_{ne}=6.6\times 10^3$ m	$L_{ne}=1.32$ m
Impurity density gradient length	$L_{nz}=-0.18$ m	$L_{nz}=1.43$ m
Trapped fraction	$f_t=\sqrt{2r/R}=0.36$	$f_t=\sqrt{2r/R}=0.62$

the X_4 component which is $e\phi_k/T_e$ and write the eigenvector as the independent $\boldsymbol{X}=(e\phi_k/T_e)\hat{\boldsymbol{X}}$. Then the components of $\hat{\boldsymbol{X}}$ are

$$\hat{\boldsymbol{X}}=\begin{bmatrix} \frac{\delta n_i}{n_e}/\frac{e\phi}{T_e} \\ \frac{\delta n_z}{n_e}/\frac{e\phi}{T_e} \\ \frac{\delta n_e}{n_e}/\frac{e\phi}{T_e} \\ 1 \end{bmatrix}. \tag{33}$$

Physically, the $\hat{\boldsymbol{X}}$ vector describes the "polarization" of density waves related to the electrostatic potential wave of plasma oscillations. Now the quasilinear particle fluxes are given by

$$\Gamma_i=\mathrm{Re}\sum_k \frac{ik_y\phi_k^*}{B}\delta n_i=-n_e\frac{T_e}{eB}\sum_k \frac{k_y|e\phi_k|^2}{T_e^2}\mathrm{Im}\,\hat{X}_1(k),$$

$$\Gamma_z=\mathrm{Re}\sum_k \frac{ik_y\phi_k^*}{B}\delta n_z=-n_e\frac{T_e}{eB}\sum_k \frac{k_y|e\phi_k|^2}{T_e^2}\mathrm{Im}\,\hat{X}_2(k), \tag{34}$$

$$\Gamma_e=\mathrm{Re}\sum_k \frac{ik_y\phi_k^*}{B}\delta n_e=-n_e\frac{T_e}{eB}\sum_k \frac{k_y|e\phi_k|^2}{T_e^2}\mathrm{Im}\,\hat{X}_3(k).$$

We have analytically and numerically verified that the first row of $A_{i,j}X_j=0$ gives that $\Gamma_e=\Gamma_i+Z\Gamma_z$. The flux formulas in Eq. (34) are ambipolar with $\Gamma_i+Z\Gamma_z=\Gamma_e$. The quasilinear formulation in Eq. (34) is valid when there are overlapping resonances in the Hamiltonian motion of the test particles.[9,10] The conditions are given in Ref. 8. In the nonlinear state the fastest growing modes couple to the damped eigenmodes driving them up to the level required for the power flow from the unstable waves to balance the damping from the stable modes.

The nonlinear waves will saturate when the finite k_x part of the spectrum grows up to have the rms values of $\delta n_i/n_i\sim Z\delta n_z/n_e\sim \rho_\tau/\langle k_x^2L_n^2\rangle^{0.5}$. The spectrum has an isotropic part at higher $k_\perp$ and a zonal flow and density flattening part at low k_y values. There are coherent vortices that come and go in the turbulence and are especially strong in the limit of small parallel diffusivity $\nu_\parallel\ll|\omega_k|$. The turbulent wavenumber spectrum that enters Eq. (34) is modeled as[11]

$$\left|\frac{e\phi_k}{T_e}\right|^2=\frac{I_0}{(1+k_\perp^2\rho_s^2)^2}, \tag{35}$$

where I_0 is the constant value determined by the rms fluctuations.

For higher $k_y\rho_s$ modes the wave frequency ω_k can change direction from the electron to the ion diamagnetic drift direction. With this change, the net impurity particle flux can also change direction. To determine the magnitude and direction of the hydrogen and impurity flux we need eigenvectors determined by Eq. (34).

Figure 3 gives the phase shifts in radians of hydrogenic ion, impurity, and electron densities from the electrostatic potential fluctuations ϕ_k as a function of poloidal wave number k_y. The phase shifts of the collisional drift wave system and the trapped electron mode are computed from the matrices of Eqs. (24) and (28), respectively. Figures 3(a) and 3(b) show the phase shifts of the collisional drift wave model at $r/a=0.2$ and $r/a=0.6$, respectively. Figure 3(c) shows the phase shifts of the trapped electron mode at $r/a=0.6$. There

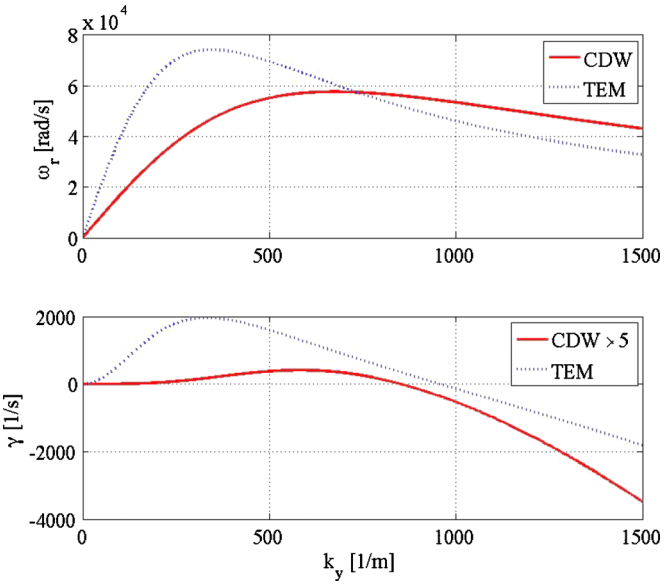

FIG. 2. (Color online) Real frequency ω_r and the growth rate γ of the system of (solid lines) collisional and (dotted lines) trapped electron drift waves at $r/a=0.6$.

is no significant phase shift between electron density and the potential in the collisional drift wave model at $r/a=0.2$ [Fig. 3(a)]. In other words, the adiabaticity of electron motion is high enough to give the Boltzmann response. In the core, the electron temperature is higher than that in the edge plasma. The high temperature yields high electron velocity v_e which gives the Boltzmann response. Therefore, the electron quasilinear flux is small. At the normalized radius $r/a=0.6$ and with the collisional drift wave model which is shown in Fig. 3(b), the phase shifts between ion density fluctuations and the electrostatic potential fluctuations are significant. The large particle flux occurs at the $r/a=0.6$ [Fig. 3(b)]. The phase shifts come from the electron-ion collisions. In the edge plasma, the electron temperature is low. Therefore, the Boltzmann response is no longer effective. The phase shifts of the trapped electron mode show a different character from the ones of the collisional drift wave [Fig. 3(c)]. The phase shifts between the ion density fluctuations and the electrostatic potential fluctuations start from $\pi/2$. The large phase shifts give the large particle fluxes for given fluctuation intensity $|\phi_k|^2$.

Figure 4 shows the quasilinear flux of the impurity (boron) for the normalized radius of $r/a=0.2$ (hollow boron density profile $L_{nz}=-0.18$ m) and $r/a=0.6$ (flat boron density profile $L_{nz}=1.43$ m). Figures 4(a) and 4(b) show the quasilinear flux of the collisional drift wave model at $r/a=0.2$ and $r/a=0.6$, respectively. Figure 4(c) shows the quasilinear flux of the trapped electron mode at $r/a=0.6$. The quasilinear fluxes are calculated for $0.1\ \mathrm{m}^{-1}<k_y<1000\ \mathrm{m}^{-1}$. The magnitude of the particle flux is different between the positions of $r/a=0.2$ [Fig. 4(a)] and $r/a=0.6$ [Fig. 4(b)]. The flux of $r/a=0.6$ [Fig. 4(b)] is ten times larger than the one of $r/a=0.2$. The intensity of the particle flux is linked with the phase shifts which were shown in Fig. 3. Figure 4(c) shows the quasilinear flux of the trapped electron mode case. The phase shifts of the particles are strong for

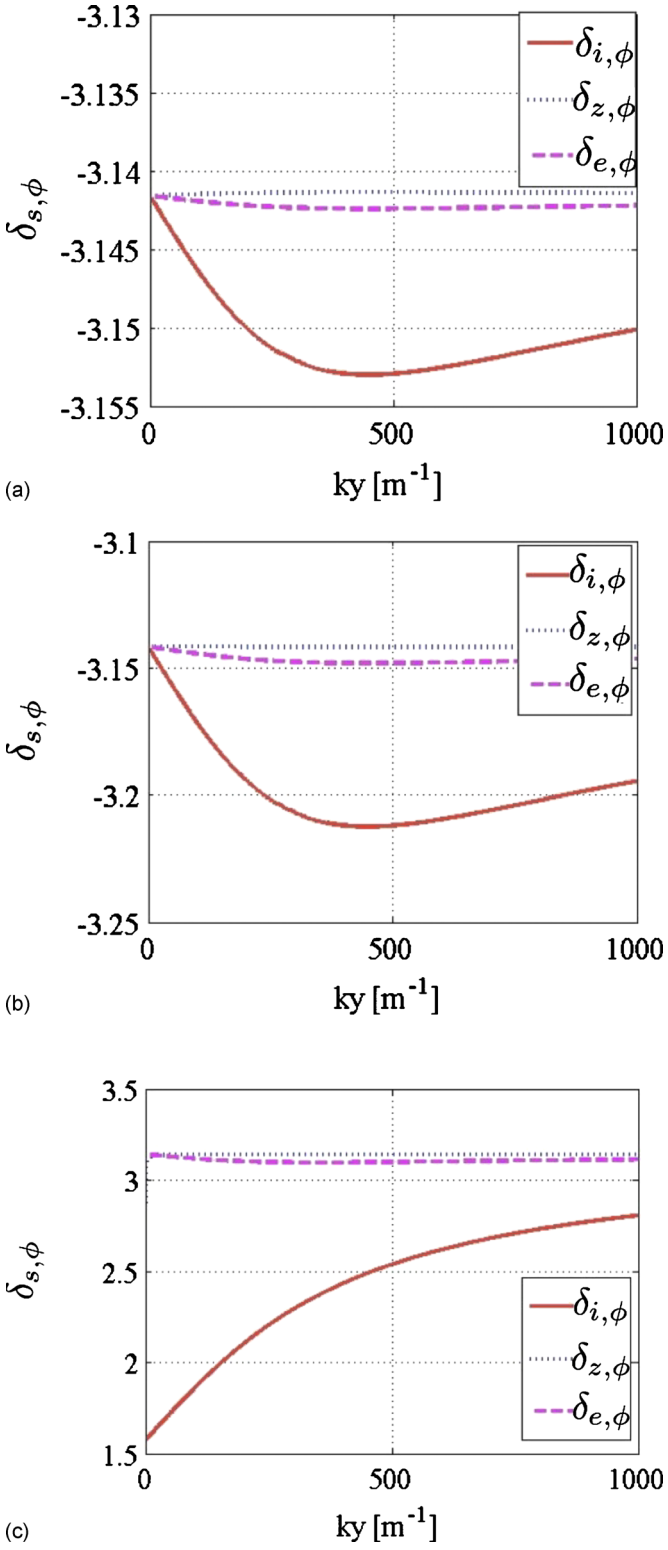

FIG. 3. (Color online) Phase shifts in radians with between hydrogenic ion, impurity, and electron densities and the electrostatic potential fluctuations ϕ as a function of k_y. (a) $r/a=0.2$, (b) $r/a=0.6$, and (c) $r/a=0.6$ of trapped electron mode.

low wavenumbers $\pi/2$ as shown in Fig. 3. Similarly, the particle flux of trapped electron mode is strong in the low wave numbers ($k_y=1-3\ \mathrm{m}^{-1}$) as shown in Fig. 4(c). Another remark is a dependence in the direction of the impurity flux Γ_z. The quasilinear fluxes of impurity densities at $r/a=0.2$

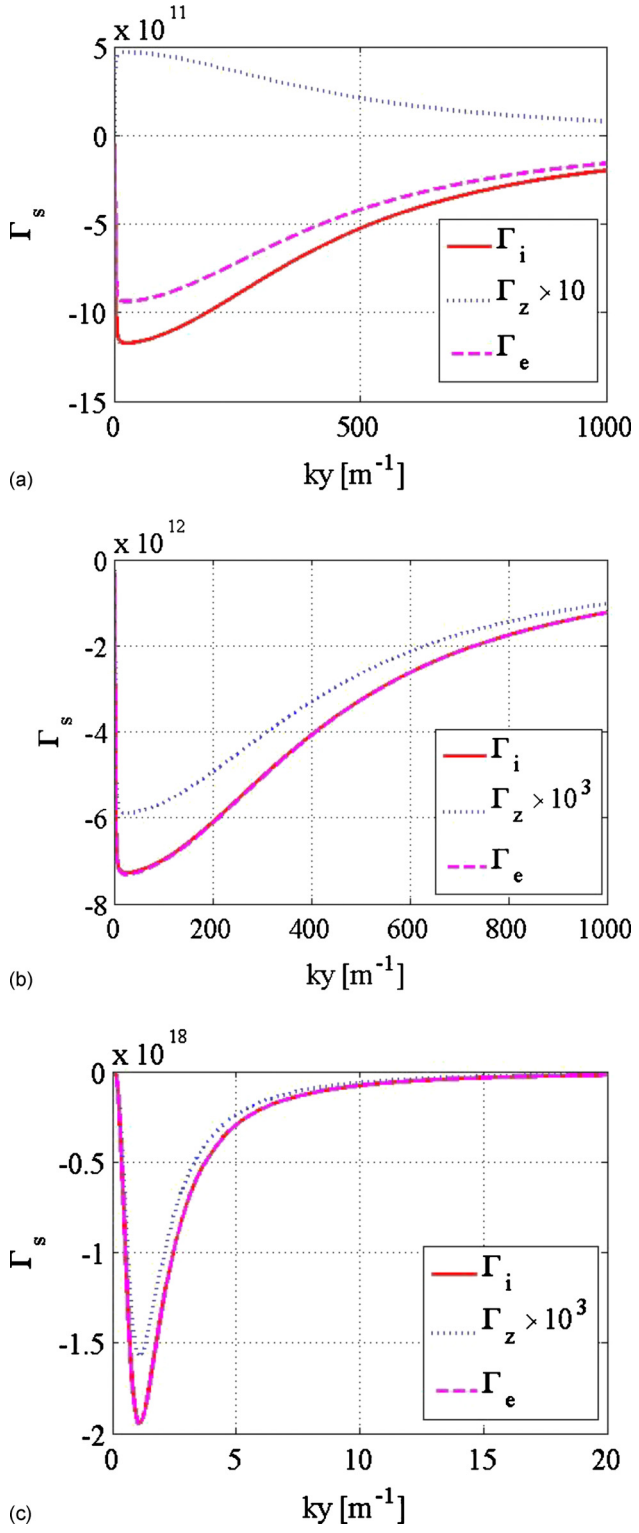

FIG. 4. (Color online) Quasilinear fluxes of boron (B) for (a) hollow impurity density profile $L_{nz}=-0.18$, (b) peaked impurity density profile $L_{nz}=1.43$, and (c) peaked impurity density profile case of trapped electron mode. The unit of the flux is ions/$(\mathrm{m}^2\ \mathrm{s}^{-1})$.

show negative value which indicates that they are inward flux. Let us note that the inward flux of the impurity density tends to accumulate impurities in the core plasma. In the hollow impurity density profiles at $r/a=0.2$, the direction of the flux reverses to be in the outward direction which is

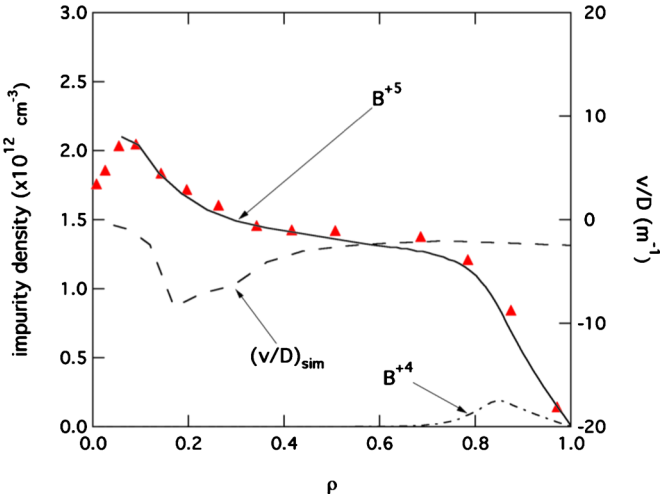

FIG. 5. (Color online) Simulation of B^{5+} density (solid line) and B^{4+} density (dashed-dotted line) compared with the measured B^{5+} density (Δ). v/D (dashed line) required in the simulation is plotted on the right axis.

favorable to fusion plasma since it expels the impurities from the core plasma.

The radial profiles of the fully striped B^{5+} ion density is known from charge exchange recombination spectroscopy for several time periods and are described in detail in Ref. 12. The internal transport barrier (ITB) for these discharges has peaked particle profiles. This particular ITB discharge does not display a significant change in the temperature profiles because of increased radiation although there is a clear improvement in the energy confinement. The temperature does not increase its peaking because of compensating increases in plasma radiation due to peaked impurities and fueling ion peaking. The analysis of sawtooth data on the soft x-ray emission has shown that there is a significant delay in the propagation of the heat pulse which occurs at the sawtooth crash across the barrier region.[13] Note also that if the temperature response is only in the ion channel, then the strong electron-ion coupling in these shots will hold down a temperature response. Figure 5 shows the measured density profile for the fully stripped boron impurity which is monotonically decreasing from 2×10^{12} cm^{-3} in the core to negligible at the scrape-off-layer (SOL). Also shown is the lower density peaked profile of the hydrogen-like B^{4+} ions. This density peaks at $\rho=0.8$, where $n(B^{4+})\sim2\times10^{11}$ cm^{-3}. The ratio of the inferred value of (v_z/D_z) is shown and inward with value approximately -3 m^{-1} while the gyro-Bohm estimate of the $v_{gB}/D_{gB}\sim5$ m^{-1}.

For contact between the theory and the data we show that the model predicts the Gaussian-like profile that is hollow for the H-mode with its peak near the maximum of the ionization source of the impurity. We note that for low ionization states such as B^{4+} the $dn_z/dr>0$ while for fully stripped B^{5+} the gradient is $dn_z/dr<0$. For this regime, the convection part of the impurity flux is outward $V>0$. For the later phase ITB regime driven by the ion cyclotron resonance frequency heating we find that the theory predicts the observed peaked profile from a small negative or inward convection velocity. The convection velocity is small and sensi-

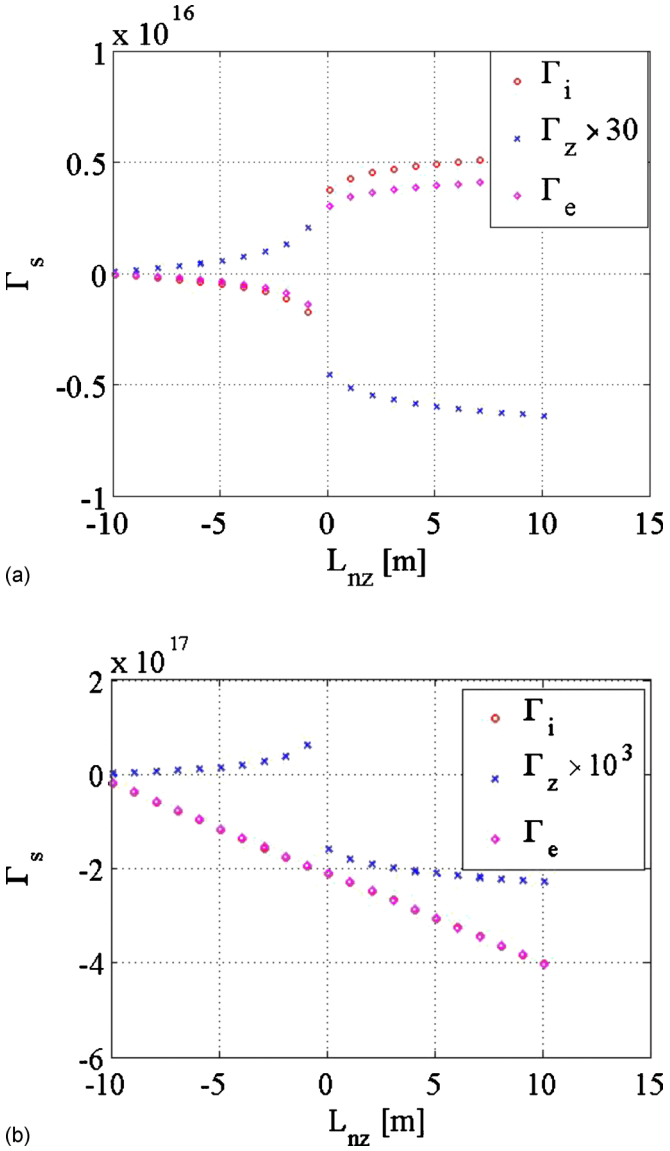

FIG. 6. (Color online) Quasilinear fluxes of boron (B) as dependence of impurity density length L_{nz} for (a) $L_{ne}=6.6\times10^3$ m and (b) $L_{ne}=1.32$ m. The unit of the flux is ions/$(m^{-2}\ s^{-1})$.

tive to the details of the system parameters and gradient scale lengths. Models for the peaked and hollow impurity profiles are derived and when fit to the B^{5+} data give the ratio of the V/D values. The collisionality regime and the gradients considered here are taken from the Alcator C-Mod data for shot No. 1070831028 provided by the Alcator C-Mod team. (See Appendix A for this discussion.)

There is a reversal of the fluxes of impurities under some conditions. Obviously, reversal of a flux of impurities is of critical importance. Figure 6 shows the quasilinear fluxes Γ_s versus impurity density scale length L_{nz} with a frame (a) showing the case for flat H-mode-like electron density profile ($L_{ne}=6.6\times10^3$ m at $r/a=0.2$) and (b) showing the case for peaked electron density profile ($L_{ne}=1.32$ m at $r/a=0.6$). The region around $L_{nz}=0$ has the impurity gradient passing through infinity. We see the important change in the direction of the sign of the impurity flux going through this region. Positive impurity density gradient scale lengths indicate that impurity density is a peaked profile. In the peaked impurity density profile, the impurity flux is directed inward which leads to impurity accumulation in the core plasma. Similarly, the negative impurity density gradient scale lengths indicate that impurity density is a hollow profile. A hollow impurity density profile leads to a reversal in the direction of the impurity flux, creating an outward flow that is favorable for the fusion plasma since it expels impurities from the core plasma.

Another remark concerns the reversal of fluxes of the electrons and ions. For the large density gradients $L_{ne}=6.6\times10^3$ m, the reversal of the fluxes of the electrons and ions accompanies the reversal of the flux of the impurities, as shown in Fig. 6(a). When the impurity scale length is negative, $L_{nz}<0$, the fluxes of the electron and ions are directed inward while the impurity scale length is positive, $L_{nz}>0$, the fluxes of the electron and ions are directed outward. However, for low density gradients $L_{ne}=1.32$ m, the direction of the fluxes of the electrons and the ions do not change, i.e., the fluxes are always in inward direction, as shown in Fig. 6(b). In this case, the flux of the electrons and ions are not affected by the impurities.

VI. THEORETICAL ESTIMATIONS

Impurity density n_z influences the turbulent transport. In this section, an estimation of the dependence of impurity density on quasilinear flux is discussed.

Let us consider the pure plasma $n_z=0$ and $n_i=n_e$ as an initial condition. Impurities will be gradually injected up to $n_e=Zn_z$. Figure 7 shows the quasilinear flux as a function of impurity density n_z for (a) peaked impurity density profile ($L_{nz}=0.18$ m>0) and (b) hollow impurity density profile ($L_{nz}=-0.18$ m<0). In the state of low impurity density ($n_z<10^{17}$), the ion and electron fluxes are $\Gamma_i\sim\Gamma_e\sim-3\times10^{16}$ ions/$m^2\ s^{-1}$. The calculations of the quasilinear flux are performed with Eq. (34) for wavenumbers of k_x and k_y up to 2000 m^{-1}.

Figure 8 compares the quasilinear flux of boron and argon as a function of impurity density n_z. The impurity density gradient L_{nz} is fixed as $L_{nz}=0.18$ m for peaked impurity density profile and $L_{nz}=-0.18$ m for the hollow impurity density profile. The results indicate that the quasilinear flux of the heavy impurity is smaller than the flux of the light impurity.

VII. CONCLUSIONS AND FUTURE DIRECTIONS

In this work on impurity transport in toroidal plasmas we have derived and solved two systems of drift wave turbulence equations for the three-component plasma with hydrogenic ions and a single species of impurity ions. We have formulated the problem in a way that makes it clear how to generalize the system to that for multiple impurity species. We applied the model to the boron impurity data from the Alcator C-Mod experiments.

In the SOL we generalize the familiar Hasegawa–Wakatani model with cold ions and isothermal electrons to acquire the eigenmodes in the three-component plasma system. The nonlinear system for the collisional drift wave is

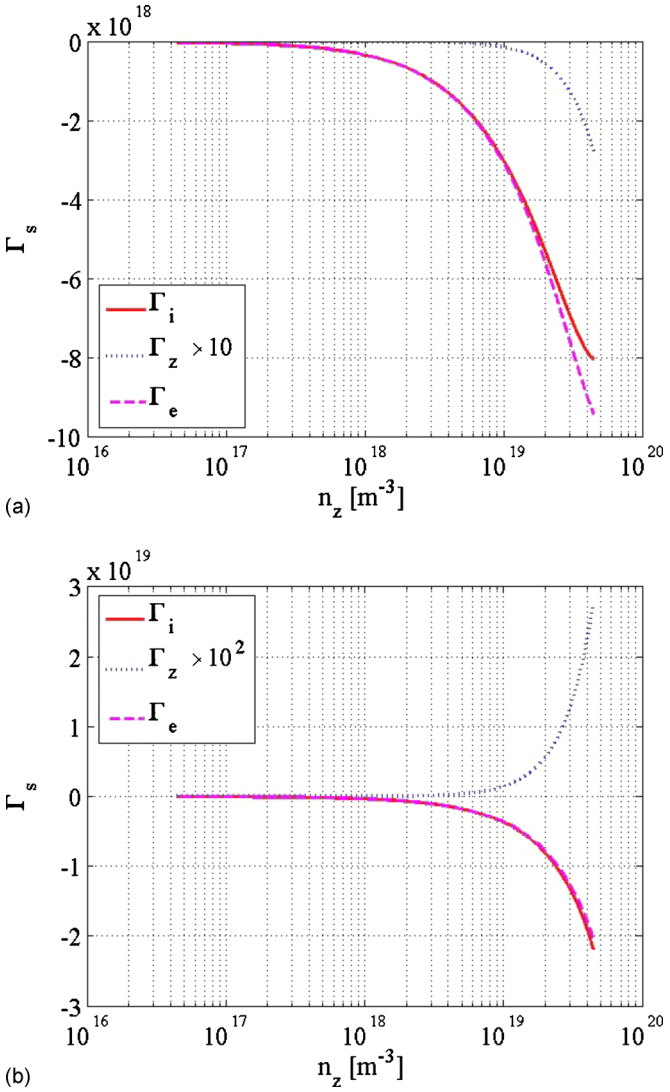

FIG. 7. (Color online) Quasilinear flux as a function of n_z. (a) Peaked impurity density profile $L_{nz}=0.18$ m>0 and (b) hollow impurity density profile $L_{nz}=-0.18$ m<0.

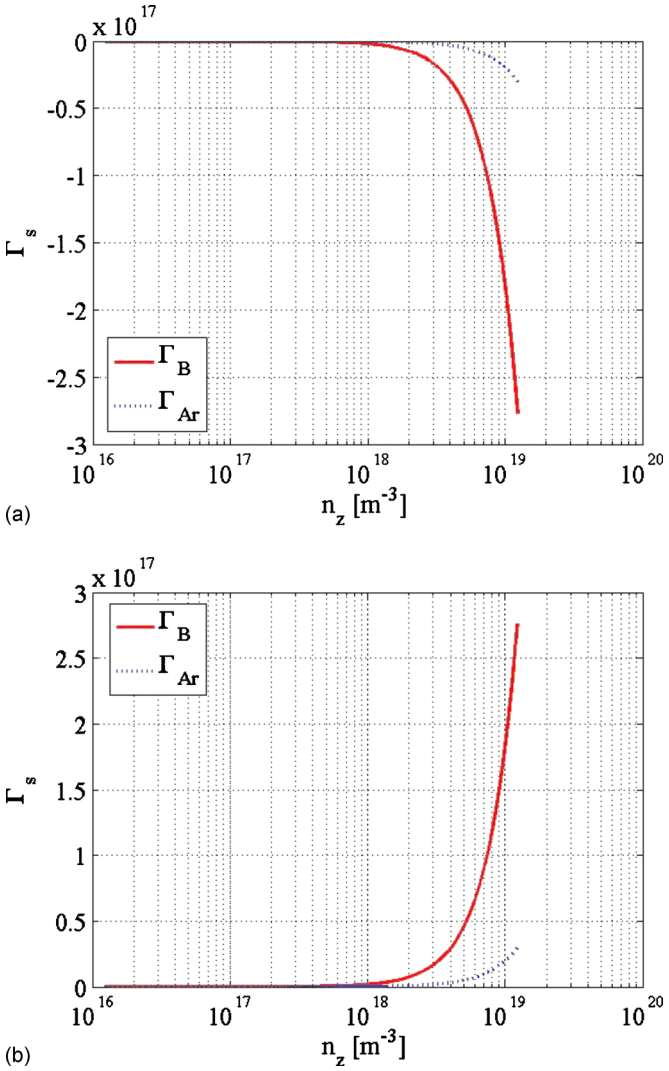

FIG. 8. (Color online) Comparison of quasilinear flux of boron (Γ_B) and argon (Γ_{Ar}) as a function of n_z. (a) peaking profile $L_{nz}=0.18$ m>0 and (b) hollow profile $L_{nz}=-0.18$ m<0.

given in Eq. (4) and the linear and quasilinear solutions have been discussed. The results show that the larger particle flux occurs at $r/a=0.6$ comparing to $r/a=0.2$ of Alcator C-Mod experiments. The analysis indicates that there are no significant phase shifts between the density and the electrostatic potential at $r/a=0.2$ while the large phase shifts exist at $r/a=0.6$. The phase shifts are linked with the particle fluxes, i.e., when the phase shifts are large, the particle flux is large, and when the phase shift is small, the particle flux is small.

Inside the SOL or separatrix the relevant turbulence is the trapped electron mode and we use the Horton *et al.*[14] (1980) formulation of the basic Kadomtsev–Pogutse[7] (1970) model to formulate this turbulence. We simplify the analysis by neglecting all temperature gradients and derive a mathematical structure similar to that of the collisional drift waves with the trapped electron density having nonlinear dynamical equation while the passing electrons behave adiabatically. The results of quasilinear flux analysis indicate that the low wavenumbers are dominant for the particle fluxes. This is caused by the large phase shifts in the low wave numbers. The comparison of the results of the trapped electron mode and the collisional drift case indicates that the trapped electron mode has higher frequency and turbulence intensity than those of the collisional drift wave. The strong turbulence gives rise to coherent structures.

The results show that freeing up of the hydrogenic density from the constraint that it is exactly equal to the electron density in the two-component plasma allows the dynamics of the impurities species to increase the richness of the turbulence. A significant concentration of high Z impurities alters the turbulence properties and turbulent transport. Similarly, a light concentration of low Z impurities behave like passive tracers. In other results, a hollow impurity density profile leads to a reversal in the direction of the impurity flux, creating an outward flow that is favorable for the fusion plasma since it expels impurities from the core plasma. This work may lead to new strategies for controlling impurity transport.

Further work needs to be done to expand nonlinear study and to determine how the coherent structures and zonal flows impact the quasilinear predictions for the transport of fluxes.

Coherent structures are outside the domain of applicability of the quasilinear theory. For transport modeling, however, the quasilinear fluxes with conventional models or data for the wave amplitudes and the spectral index of the turbulence may provide useful formulation for integrated systems modeling of fusion power systems. The eigenmodes diagonalize the complex linear matrices and thus are critically important for determining the relative amounts of transport in the hydrogenic and impurity fluxes. The nonlinear interactions of the growing eigenmodes with the damped eigenmodes determine the spectral densities as modeled with a simple parametrization. In Appendix B we give the formulation of the dynamical equations describing the interaction of the eigenmodes. The formulation maybe used to write low order models of the dynamics which often gives insight to the nonlinear dynamics of the partial differential equations.

ACKNOWLEDGMENTS

S.F. acknowledges Université de Provence for the fellowship. This work was supported by the U.S. Department of Energy Center supported by USDOE under Award No. DE-FG03-96ER54373, International Institute for Fusion Science, and the CEA at Cadarache. Dr. X. Garbet and Dr. R. Guirlet gave the fruitful comments from the view point of experiment on this work. Useful discussion with Dr. D. del-Castillo-Negrete is also acknowledged on the breakdown of the quasilinear formulation for regions surrounding the internal transport barriers. The authors thank the Alcator C-Mod team for the data provided for this impurity transport study.

APPENDIX A: ATOMIC PROCESSES OF THE IMPURITIES

The source of B^{5+} is from the ionization of B^{4+} which couples to $n_5=n_{z=5}$ to $n_4=n_{z=4}$ through the ionization rate $n_e S_4(T_e)$ and recombination rate $n_e\alpha_5(T_e)$. To solve the transport problem with the source and the sink, we write

$$\frac{\partial n_5}{\partial t}+\boldsymbol{v}_E\cdot\nabla n_5=n_e(S_4n_4-\alpha_5n_5), \tag{A1}$$

$$\frac{\partial n_4}{\partial t}+\boldsymbol{v}_E\cdot\nabla n_4=n_e(S_3n_3-\alpha_4n_4-S_4n_4+\alpha_5n_5). \tag{A2}$$

There is a large energy gap between the binding energy of $n(B^{4+})$ and $n(B^{5+})$ so that the coupling to the lower states of ionization can be neglected.

Averaging Eqs. (A1) and (A2) over the turbulence gives

$$\frac{\partial n_5}{\partial t}+\frac{1}{r}\frac{\partial}{\partial r}(r\Gamma_5)=n_e(S_4n_4-\alpha_5n_5), \tag{A3}$$

$$\frac{\partial n_4}{\partial t}+\frac{1}{r}\frac{\partial}{\partial r}(r\Gamma_4)=n_e(S_3n_3-\alpha_4n_4-S_4n_4). \tag{A4}$$

Since S_4n_4 is large compared with α_5n_5 in the region $T_e\approx 100$ eV we find that the steady flux is

$$\Gamma_5(r)=-\frac{1}{r}\int_r^a dr' r' n_e n_4 S_4. \tag{A5}$$

For r less that the radius of the scrape-off-layer r_{SOL}, the integral becomes a constant.

From Eq. (A5) we calculate the flux Γ_5. When Γ_5 is positive or negative, it indicates that the n_5 profile is time evolving. For a steady state, the flux is $\Gamma_5=0$. With $V_5=(r/r_1)V$ and a constant diffusion coefficient D and pinch velocity V we show that the B^{5+} profile is peaked for inward $V<0$ with

$$n_5(r)=n_5(0)\exp\left(-\frac{|V|r^2}{2r_1D}\right) \tag{A6}$$

and is hollow for $V>0$ with

$$n_5(r)=n_5(0)\exp\left(-\frac{|V|(a^2-r^2)}{2r_1D}\right) \tag{A7}$$

for simple boundary condition. Here, r_1 is a characteristic radius inside the ionization layer.

The transport dynamics analysis has been studied with the ionization source term $n_e n_{B^{4+}}\langle\sigma v_e\rangle$ that peaks near the ionization energy $T_e=340$ eV region of B^{4+} source. With the source term included we are able to estimate D and V separately and find that typical values are 0.1 $\mathrm{m^2\,s^{-1}}$ and $V\leq 100$ $\mathrm{m\,s^{-1}}$.

APPENDIX B: SPECTRAL EXPANSION OF THE NONLINEAR FIELDS

Owing to the complex dependence of dynamics on the linear equations of matrix, this is not the standard form of Hamiltonian systems. So we introduce the left $\boldsymbol{y}_i^*=\langle i|$ and the right $\boldsymbol{x}_j=|j\rangle$ eigenvectors of the auxiliary matrix $\boldsymbol{M}=\boldsymbol{B}^{-1}\boldsymbol{A}$. The left eigenvectors are taken from

$$\boldsymbol{y}_i^*\boldsymbol{M}=\lambda_i\boldsymbol{y}_i^* \tag{B1}$$

and the right eigenvectors are taken from

$$\boldsymbol{M}\boldsymbol{x}_j=\lambda_j\boldsymbol{x}_j. \tag{B2}$$

Then postmultiply (B1) by $\boldsymbol{x}_j$ and subtracting from premultiply (B2) by $\boldsymbol{y}_i^*$ leads to

$$(\lambda_j-\lambda_i)\boldsymbol{y}_i^*\boldsymbol{x}_j=0 \tag{B3}$$

from which we claim $\langle i|j\rangle=\boldsymbol{y}_i^*\boldsymbol{x}_j=0$ for nondegenerate $\lambda_i\neq\lambda_j$ eigenvalues of the two problems, Eqs. (B1) and (B2). Now we can normalize $\langle i|i\rangle=1$ and proceed as in quantum mechanical perturbation theorem.

We now expand the turbulent fluctuation in terms of the eigenvectors of the linear system. The advantage of the eigenmode expansion over that of Fourier modes is that the linear coupling is taken into account exactly. The evolution of the expansion coefficient $C_{k,i}(t)$ is due entirely to the nonlinear interactions. Conceptually, the formulation is that of the early plasma turbulence work of Galeev and Sagdeev.[15,16]

The vector field $\boldsymbol{X}(t)$ is expressed as the sum over a set of k_x,k_y,k_z modes and for each $\boldsymbol{k}$ mode, there is a sum over the three distinct eigenmodes, $j=1,2,3$. We define the time dependent expansion coefficients that

$$X(t) = \sum_{j,\boldsymbol{k}} C_{\boldsymbol{k},j}(t) X_j e^{i\boldsymbol{k}\cdot\boldsymbol{x} - i\omega_{\boldsymbol{k},j} t} + \text{c.c.}, \tag{B4}$$

where the dynamics $dC_{\boldsymbol{k},j}/dt$ is due to the nonlinear terms in Eqs. (4) and (22).

Substituting into Eq. (B4) we find

$$\sum_{\boldsymbol{k},j} \left(\omega C_{\boldsymbol{k},j} + i \frac{dC_{\boldsymbol{k},j}}{dt} \right) B X_{\boldsymbol{k},j} e^{i\boldsymbol{k}\cdot\boldsymbol{x} - i\omega_j t} = \sum_{\boldsymbol{k},j} A(\boldsymbol{k}) C_{\boldsymbol{k},j} X_j + \sum_{\boldsymbol{k}',j'} \sum_{\boldsymbol{k}'',j''} N(X_{\boldsymbol{k}'}, X_{\boldsymbol{k}''}) C_{\boldsymbol{k}',j'} C_{\boldsymbol{k}'',j''}. \tag{B5}$$

Now multiplying through Eq. (B5) by $\boldsymbol{B}^{-1}$ and contracting, or projecting, the equation onto the left eigenvector $\boldsymbol{Y}_{l,\boldsymbol{k}''} = \langle l, \boldsymbol{k}'' |$ yields as

$$\sum i \langle Y_{l,\boldsymbol{k}''} | X_{l,\boldsymbol{k}} \rangle \frac{dC_{l,\boldsymbol{k}}}{dt} = \sum_{m,\boldsymbol{k}_1,n,\boldsymbol{k}_2} \langle Y_{l,\boldsymbol{k}} | N(X_{m,\boldsymbol{k}_1}, X_{n,\boldsymbol{k}_2}) C_{m,\boldsymbol{k}_1}(t) C_{n,\boldsymbol{k}_2}(t) \times \exp\{ i(\omega_{\boldsymbol{k}} - \omega_{\boldsymbol{k}_1} - \omega_{\boldsymbol{k}_2}) t \}. \tag{B6}$$

We normalize the diagonal terms of such that $\langle Y_{l,\boldsymbol{k}''} | X_{l,\boldsymbol{k}} \rangle = \delta_{l,\boldsymbol{k}}$. Then we arrive at the nonlinear dynamical equation as given as

$$i \frac{dC_{l,\boldsymbol{k}}}{dt} = \sum_{\boldsymbol{k}'+\boldsymbol{k}''=\boldsymbol{k},l,m,n} \langle Y_{l,\boldsymbol{k}} | N | X_{m,\boldsymbol{k}_1}, X_{n,\boldsymbol{k}_2} \rangle C_{m,\boldsymbol{k}_1}(t) C_{l,\boldsymbol{k}_2}(t) \times \exp\{ i(\omega_{\boldsymbol{k}} - \omega_{\boldsymbol{k}_1} - \omega_{\boldsymbol{k}_2}) t \}. \tag{B7}$$

Equation (B7) is of the same form that occurs in quantum mechanics for the phonon-phonon interactions with a summation of the $\boldsymbol{k}$-space lattice and a second summation over in state j. In the plasma problem the matrices are not Hamiltonian. The interactions come in resonant **k**-vector triads but contain the additional complexity of each triad having three degrees of freedom for the interaction within each triad.

[1] K. J. Dietz and JET Team, Plasma Phys. Controlled Fusion **32**, 837 (1990).
[2] M. Shimada, D. J. Campbell, V. Mukhovatov, M. Fujiwara, N. Kirneva, K. Lackner, M. Nagami, V. D. Pustovitov, N. Uckan, J. Wesley, N. Asakura, A. E. Costley, A. J. H. Donne, E. J. Doyle, A. Fasoli, C. Gormezano, Y. Gribov, O. Gruber, T. C. Hender, W. Houlberg, S. Ide, Y. Kamada, A. Leonard, B. Lipschultz, A. Loarte, K. Miyamoto, V. Mukhovatov, T. H. Osborne, A. Polevoi, and A. C. C. Sips, Nucl. Fusion **47**, S1 (2007).
[3] A. Hasegawa and M. Wakatani, Phys. Rev. Lett. **50**, 682 (1983).
[4] P. W. Terry and W. Horton, Phys. Fluids **26**, 106 (1983).
[5] M. Greenwald, R. L. Boivin, F. Bombarda, P. T. Bonoli, C. L. Fiore, D. Garnier, J. A. Goetz, S. N. Golovato, M. A. Graf, R. S. Granetz, S. Horne, A. Hubbard, I. H. Hutchinson, J. H. Irby, B. LaBombard, B. Lipschultz, E. S. Marmar, M. J. May, G. M. McCracken, P. O'Shea, J. E. Rice, J. Schachter, J. A. Snipes, P. C. Stek, Y. Takase, J. L. Terry, Y. Wang, R. Watterson, B. Welch, and S. M. Wolfe, Nucl. Fusion **37**, 793 (1997).
[6] W. Horton, Phys. Fluids **19**, 711 (1976).
[7] B. B. Kadomtsev and O. P. Pogutse, "Turbulence in toroidal systems," in *Reviews of Plasma Physics*, edited by M. A. Leontovich (Consultants Bureau, New York, 1970), vol. 5, p. 94.
[8] W. Horton and Y.-H. Ichikawa, *Chaos and Structures in Nonlinear Plasmas* (World Scientific, Singapore, 1996), p. 340.
[9] Y. Elskens and D. F. Escande, *Macroscopic Dynamics of Plasmas and Chaos* (IOP, Bristol, 2003), p. 94.
[10] D. del-Castillo-Negrete, J. M. Greene, and P. J. Morrison, Physica D **91**, 1 (1996).
[11] W. Horton, X. N. Su, and P. J. Morrison, Sov. J. Plasma Phys. **16**, 562 (1990).
[12] W. L. Rowan, I. O. Bespamyatnov, and C. L. Fiore, Nucl. Fusion **48**, 105005 (2008).
[13] C. L. Fiore, P. T. Bonoli, D. R. Ernst, A. E. Hubbard, M. J. Greenwald, A. Lynn, E. S. Marmar, P. Phillips, M. H. Redi, J. E. Rice, S. M. Wolfe, S. J. Wukitch, and K. Zhurovich, Phys. Plasmas **11**, 2480 (2004).
[14] W. Horton, D. I. Choi, P. Terry, and D. Biskamp, Phys. Fluids **23**, 590 (1980).
[15] A. A. Galeev and R. Z. Sagdeev, J. Exp. Theor. Phys. **26**, 233 (1968).
[16] A. A. Galeev and R. Z. Sagdeev, in *Reviews of Plasma Physics*, edited by M. A. Leontovich (Consultants Bureau, New York, 1973), p. 1.